Resonance Raman and FTIR Spectra of Isotope-Labeled Reduced 1,4-Benzoquinone and Its Protonated Forms in Solutions

Xiaojie Zhao,[†] Hiroshi Imahori,[‡] Chang-Guo Zhan,[†,§] Yoshiteru Sakata,[‡] Suehiro Iwata,[†] and Teizo Kitagawa*[,†]

Institute for Molecular Science, Okazaki National Research Institutes, Myodaiji, Okazaki 444, Japan, and Institute of Scientific and Industrial Research, Osaka University, Mihogaoka 8-1, Ibaraki, Osaka 567, Japan

Received: July 8, 1996[⊗]

Resonance Raman (RR) and FTIR spectra were observed for 1,4-benzoquinone (BQ) and its $^{18}O_2$ and d_4 isotopomers in their reduced states and their protonated forms, including the anion radical ($BQ^{\bullet-}$), semiquinone radical ($BQH^{\bullet}$), dianion (BQ^{2-}), and protonated anion (BQH^-) in water and acetonitrile. The reduced species were generated electrochemically, and the RR spectra were excited *in situ* at 441.6, 363.8, 351.1, 325, and 235 nm in resonance with the three lowest electronic transitions. The observed bands were assigned empirically on the basis of the observed $^{18}O_2$- and d_4-isotopic frequency shifts and depolarization ratios and further with *ab initio* MO calculations at the MP2 level. In contrast with neutral BQ, the ^{18}O atoms of $BQ^{\bullet-}$ and BQ^{2-} were rapidly exchanged with bulk water during the RR measurements for aqueous solutions. Upon reduction from BQ to $BQ^{\bullet-}$ and BQ^{2-}, the C═O stretching mode (ν_{7a} in Wilson's notation) shifts from 1639 to 1452 and 1275 cm^{-1}, respectively, while the ν_{8a} mode exhibits smaller shifts from 1666 to 1609 and 1596 cm^{-1}, respectively. The ν_{8a} and ν_{8b} separation was 293, 149, and 81 cm^{-1} for BQ, $BQ^{\bullet-}$, and BQ^{2-}, respectively, indicating that the six-membered ring increasingly approaches a benzenoid ring as reduction proceeds. These frequency changes are in qualitative agreement with those expected from the optimized bond lengths of the MO calculations. The RR spectra of BQH^- were close to that of BQ^{2-}, suggesting that the extra charges of BQ^{2-} are mainly localized on the two oxygen atoms. Three b_{3g} vibrations were resonance enhanced for $BQ^{\bullet-}$ via vibronic coupling, and this determines the symmetry of the first allowed electronic excited state to be $^2B_{3u}$ in the D_{2h} group. Assuming D_{2h} symmetry for $BQ^{\bullet-}$ predicts the presence of five polarized RR bands in the region below 1700 cm^{-1}, but nine fundamentals were observed in addition to several overtones and combinations. In addition, one band appears both in the IR and the RR spectra. Therefore, practical molecular symmetry is reduced to C_s owing to solvation.

Introduction

Quinones in biological systems serve as an active site of quinoenzymes or a coupler of electron and proton transfers in energy-transducing membranes for respiration and photosynthesis (see refs 1−4 and references therein). In the reaction-center (RC) protein complexes of photosynthetic bacteria and plant photosystem II, there are two kinds of quinones, called quinone A (Q_A) and quinone B (Q_B). Q_A and Q_B are known to work as one- and two-electron carriers, respectively, and the fully reduced Q_B is protonated to transport two protons, while the reduced Q_A ($Q_A^{\bullet-}$) is never protonated. The origin of functional differences between Q_A and Q_B remains to be elucidated. Recently, resonance Raman (RR) and Fourier transform infrared (FTIR) spectroscopies have been applied to characterize quinones in quinoenzymes[3] and RC's.[5] To draw some structural information from the spectral changes observed in such studies, it is essential to establish mode assignments of the RR and IR bands. However, the vibrational spectra of reduced quinones have not been fully analyzed yet. In order to provide basic data for the analysis of the vibrational spectra of biological quinones, we selected 1,4-benzoquinone (BQ) as a prototype of all quinones.

Vibrational spectra of neutral BQ have been extensively studied.[6−8] There have been no RR spectra reported for the dianion (BQ^{2-}) and protonated anion (BQH^-), while there are some reports on the RR spectra of the anion radical ($BQ^{\bullet-}$)[9−12] and semiquinone radical ($BQH^{\bullet}$)[13] and the IR spectra of $BQ^{\bullet-}$ and BQ^{2-}.[14] The assignments of the vibrational modes of $BQ^{\bullet-}$ were proposed from *ab initio* MO calculations,[15,16] but the results from several semiempirical and *ab initio* MO calculations on the assignments of the electronic absorption spectra of $BQ^{\bullet-}$ are somewhat controversial; the first allowed excited state is assigned to $^2B_{3u}$ by some [9,17−18] but to ^2A_u by others.[19] It is important to determine this alternative on the basis of RR characteristics. In this study, we investigated reduced BQ's including $BQ^{\bullet-}$, $BQH^{\bullet}$, BQ^{2-}, and BQH^- and their $^{18}O_2$ and d_4 isotopomers. The RR spectra of $BQ^{\bullet-}$ are assigned on the basis of the observed isotope shifts, depolarization ratios, and *ab initio* MO calculations at a higher level. The vibrational assignments are extended to BQH^- and BQ^{2-}.

Experimental Procedures

Spectroelectrochemistry of $BQ^{\bullet-}$ and BQ^{2-}. For the electrochemical generation, *in situ* electrochemical generation, and spectroscopic characterization of quinone redox products, two kinds of electrochemical cells were used. One is a thin FTIR cell reported by Nakajima *et al.*,[20] and the other is a newly designed cell for Raman and absorption measurements. In the latter, a quartz cuvette with a suitable size for RR and absorption measurements was connected to the Pyrex reaction vessel of a three-electrode configuration for constant potential electrolysis (CPE) and cyclic voltametry (CV). The reference electrode used for all CPE and CV measurements is Ag/AgCl in saturated KCl, which was sealed by Vycor glass. This electrode, contained in

* Author to whom correspondence should be addressed.
† Okazaki National Research Institutes.
‡ Osaka University.
§ Permanent address: Department of Chemistry, Central China Normal University, Wuhan 430070, People's Republic of China.
⊗ Abstract published in *Advance ACS Abstracts,* December 15, 1996.

S1089-5639(96)02009-9 CCC: $14.00

a glass tube, is combined with the main compartment through a junction tipped with a very small hole. For reduction/oxidation, CPE was performed at 0.2-V more negative or positive than the respective redox potential (E_0), predetermined by CV. The working electrode for CV is a 3-mm^2 glassy carbon electrode (ROA) and was pretreated first by polishing with a very fine powder of aluminum oxide followed by cleaning with distilled water. After several repetitions, the electrode was cleaned by acetonitrile (MeCN) of spectroscopic grade, and then, the remaining fine particles were blown away with high-pressure gas. The auxiliary electrode, made of a platinum wire, is contained in a sealed glass tube but is connected to the reaction medium through a layer of very fine glass frit. A potentiostat (Thoto Tech. Res., Model 2001/2230) equipped with an $X-Y$ recorder was used to record cyclic voltammograms and to control the bulk electrolysis.

For bulk electrolysis, the working electrode, constructed with 80-mesh platinum gauze, was placed inside the cuvette, while the reference and counter electrodes were kept separately in the main compartment. Before the start of CV or bulk electrolysis, ultrapure N_2 gas was bubbled into the solvents for 20−30 min to remove oxygen. The N_2 flow was maintained during the Raman measurements but stopped before the CV measurements.

Chemistry of BQ^{2-} and BQH^-. BQ^{2-} and BQH^- were also generated with a chemical method under anaerobic conditions as reported.[21] Briefly, BQ^{2-} was derived by putting 1,4-hydroquinone (BQH_2) into a 1 M NaOH aqueous solution of $NaBH_4$, while BQH^- was generated by putting BQH_2 into the 0.25 M Na_2CO_3−$NaHCO_3$ buffer (pH 10.8) solution of $NaBH_4$. Both BQ^{2-} and BQH^- were stable under anaerobic conditions.

Spectroscopy. UV−visible absorption and FTIR spectra were measured with a Hitachi UV3210 spectrophotometer and SHIMADZU DR-8000 FTIR spectrometer, respectively. RR spectra were excited at 441.6 and 325 nm with He−Cd lasers (Kinmon Electrics, Models CD4805R and CD3041R, respectively), at 351.1 and 363.8 nm with an Ar ion laser (Spectra-physics Model 2045) and at 235 nm. The last line was generated through frequency doubling (BBO crystal) of the 470-nm dye-laser output (Lambda Physik, FL2002) pumped by an excimer laser (Lambda Physik, EMG 103). The scattering light at right angle was passed through a filter and dispersed with a 25-cm spectrograph (Chromex 250IS) equipped with a CCD detector (PAR, OMA 4). The experimental setup for ultraviolet resonance Raman (UVRR) measurements was described previously.[22]

Chemicals. 1,4-Benzoquinone (BQ) and 1,4-hydroquinone (BQH_2) were purchased from Wako and used without further purification. The d_4-enriched 1,4-benzoquinone (d_4-BQ) was synthesized by acid-catalyzed exchange of hydroquinone followed by oxidation using lead(IV) oxide.[23] Hydroquinone (Kishida Chemicals) was deuterated with 3.4 M sulfuric acid, prepared by sulfuric acid enriched 99% in D (96% in D_2O, Isotec Inc.) and D_2O enriched 99.9% in D (Isotec Inc.), by refluxing for 36 h. After cooling, the precipitate was collected by filtration, dried, and then oxidized with lead(IV) oxide in dichloromethane at room temperature overnight. The d_4-enriched BQ was purified by sublimation. Mass spectroscopy shows that the product is 93% enriched in D. The $^{18}O_2$-isotope-enriched 1,4-benzoquinone ($^{18}O_2$-BQ) was prepared by stirring a benzene solution containing BQ with water enriched 97.1% in ^{18}O (Isotec Inc.) in a sealed tube for 9 days at room temperature according to Becker *et al.*[24] and was purified also by sublimation. The product is 80% enriched in ^{18}O, as assayed by mass spectroscopy.

Acetonitrile (MeCN) of spectroscopic grade (Dojin Chemicals) was distilled under an atmosphere of ultrapure N_2 gas just before electrochemical experiments. The supporting electrolytes used for organic solutions were freshly prepared tetrabutylammonium perchlorate (TBAP) and tetrabutylammonium tetrafluoroborate (TBAF), which were purchased from Nacalai Tesque (Kyoto, Japan), while KCl was used for aqueous solutions. $NaBH_4$, Na_2CO_3, and $NaHCO_3$ were purchased from Wako Chemicals. The pH value for 0.25 M Na_2CO_3−$NaHCO_3$ aqueous solution was determined to be 10.8 with a Beckman Q71 pH meter.

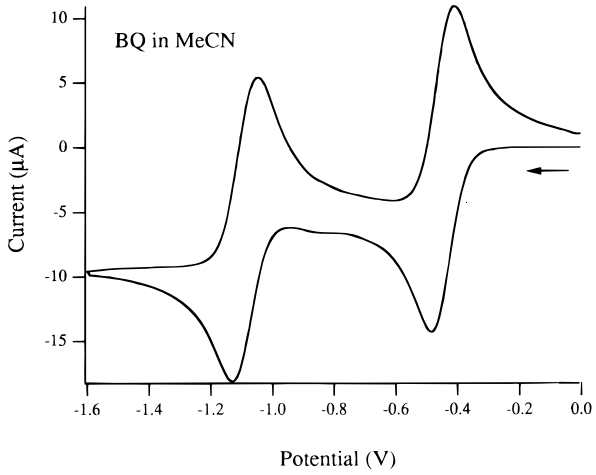

Figure 1. Cyclic voltammogram of BQ in MeCN. The concentration of BQ was 1 mM. The arrow indicates the scan direction.

***Ab Initio* MO Calculations.** The *ab initio* MO calculations for BQ, $BQ^{\bullet-}$, and BQ^{2-} were performed by the use of the MP2 method with a 631+G(d,p) basis set augmented with diffuse sp functions on the two oxygen atoms, while, practically, the Gaussian 92 package[25] on a NEC-SX3 supercomputer of this institute was used. All electrons were incorporated into the calculations of the electron correlation, while details will be described elsewhere.[26]

Results

Figure 1 shows the CV curve of BQ observed for the MeCN solution. The potentials corresponding to two pairs of negative/positive peaks were determined to be −0.46/−0.40 V vs Ag/AgCl (in saturated KCl) for the $BQ/BQ^{\bullet-}$ redox couple and −1.09/−1.03 V for the $BQ^{\bullet-}/BQ^{2-}$ couple, which agree with published results.[21] Both of the two one-electron waves were separated by 60 mV between the positive and negative scans, and the peak current for the cathodic process was equal to that of the anodic process. Thus, these redox reactions are kinetically reversible, and the two midpoint potentials (−0.43 and −1.06 V) can be regarded as the thermodynamical E_0 values.

Bauscher and Mäntele[14] attributed a very small wave between the two major peaks to the reduction of semiquinone ($QH^{\bullet}$) to protonated anion (QH^-). However, the redox potential of $QH^{\bullet}/QH^-$ should be more positive than that of $BQ/BQ^{\bullet-}$.[21] In addition, the redox potentials of the small waves were always the same for different quinones in our measurements (data not shown). Therefore, it is unlikely to ascribe it to the reduction of $BQH^{\bullet}$. On the other hand, solvated oxygen molecules exhibited a redox at the same value as that of the small wave. Moreover, the amplitude of current for the small wave decreased by the decrease of oxygen concentration in the solution. Therefore, the small wave reported is reasonably attributed to the reduction of solved oxygen in MeCN and not to the reduction of $BQH^{\bullet}$.

Figure 2 shows the UV−visible absorption spectra of $BQ^{\bullet-}$ (upper) and BQ^{2-} (lower) which were observed in water (solid

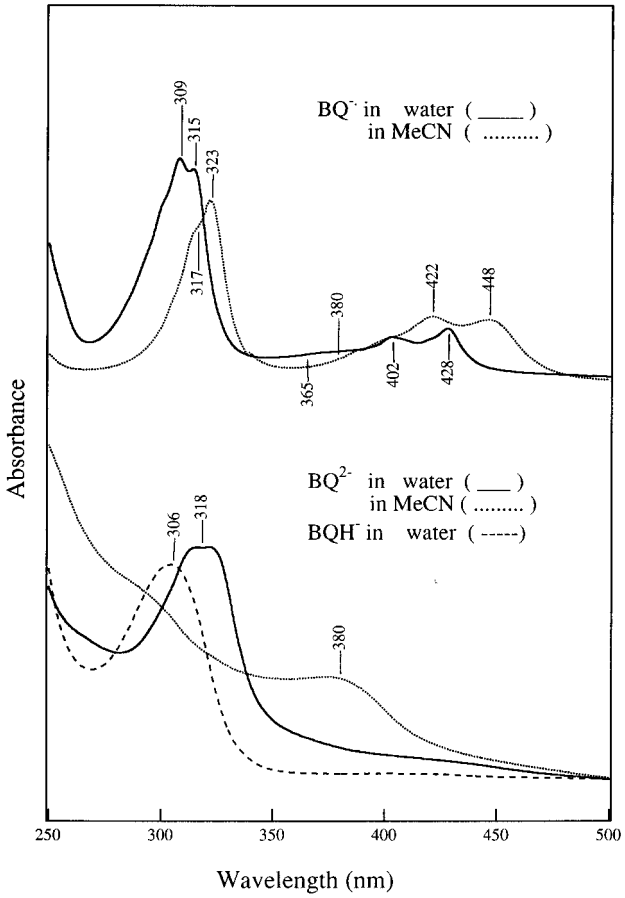

Figure 2. Uv/vis absorption spectra of $BQ^{\bullet-}$ (upper) and BQ^{2-} (lower) recorded during CPE of BQ: solid lines, in water; dotted lines, in acetonitrile; dashed lines, protonated form (BQH) in water. The initial concentration of BQ is the same for all measurements, but the effective concentrations of the species in question may not be the same.

TABLE 1: Absorption Maximum (nm) of BQ and Its Reduced Species in Water and MeCN

species	H_2O	CH_3CN
BQ	246	242
$BQ^{\bullet-}$	309, 315; ~365; 402, 428	317, 323; ~380; 422, 448
BQ^{2-}	316	380
$BQH^{\bullet}$ [a]	415	
BQH^{-}	306	
BQH_2	221; 289	225; 294

[a] Data from ref 27.

lines) and MeCN (dotted lines). The spectrum of BQH^- in water is also contained in the lower curves (dashed line). The separation between the 422- and 448-nm bands of d_4-$BQ^{\bullet-}$ in MeCN was smaller than that for $BQ^{\bullet-}$ by 20 cm^{-1} when the bands were fitted with Lorentzians, and their relative intensities were appreciably altered by deuteration of quinone (not shown). These features are in consonance with the proposal that the 422-nm band is the vibronic progression of the 448-nm transition.[9,18] Table 1 lists the wavelengths of absorption maxima of BQ, $BQ^{\bullet-}$, $BQH^{\bullet}$, BQ^{2-}, BQH^-, and BQH_2 in water and MeCN, which agree with published data.[21,27] The absorption maxima of both $BQ^{\bullet-}$ and BQ^{2-} are shifted to the blue in H_2O relative to those in MeCN, and the solvent-dependent shifts are much larger for $BQ^{\bullet-}$ and BQ^{2-} than for BQ or BQH_2.

Figure 3 shows the RR spectra of $BQ^{\bullet-}$ in MeCN (A) and water (B) excited at 441.6 nm. The bands marked by S arise from solvent. The RR spectrum of $BQ^{\bullet-}$ prepared electrochemically in an aqueous solution (B) is in agreement with those of $BQ^{\bullet-}$ derived with pulse radiolysis,[9,15] flash photolysis,[10,11]

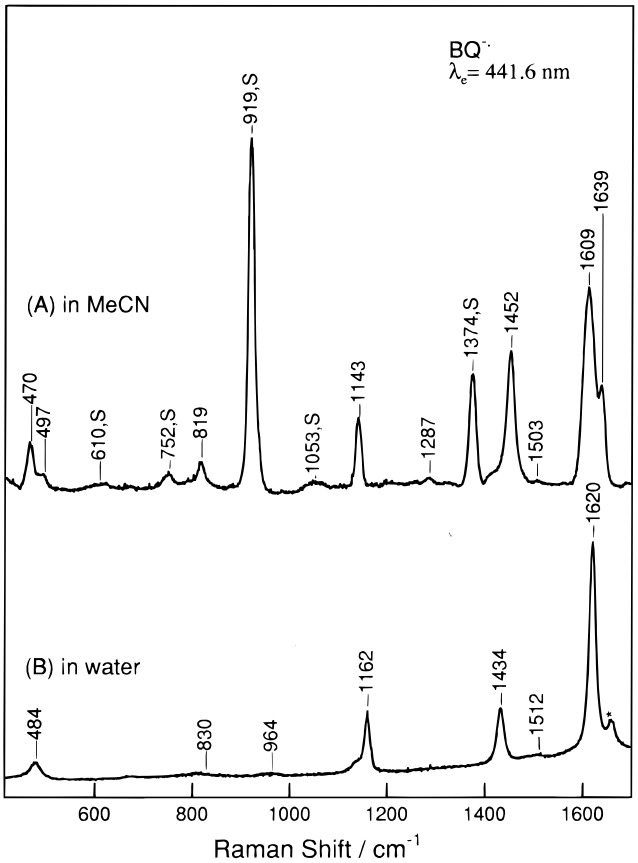

Figure 3. Resonance Raman spectra of $BQ^{\bullet-}$ in MeCN (A) and water (B) upon excitation at 441.6 nm. The bands marked by S or * are due to solvent or laser emission line, respectively. Laser power, 5 mW; accumulation time, 15 min.

and chemical methods.[12] The Raman bands at 1620 and 484 cm^{-1} in H_2O appear as if they were doublets in MeCN at 1609 and 1639 cm^{-1} and at 470 and 497 cm^{-1}, respectively, though their average frequencies are accidentally coincident with the single bands in trace B, it is not a simple case of splitting as discussed later. Note that the bands at 1434 and 1162 cm^{-1} in H_2O are shifted in opposite directions (to 1452 and 1143 cm^{-1}, respectively) in MeCN.

Figure 4 shows the RR spectra of $BQ^{\bullet-}$ in MeCN excited at 351.1 (A) and 363.8 nm (B), which are expected to appear in resonance with the second transition around 380 nm. The doublet component at 1639 cm^{-1} in Figure 3A disappeared in Figure 4, but the split component at 497 cm^{-1} in Figure 3A was relatively intensity-enhanced upon excitation at 351.1 nm. Thus, the individual bands in the doublet behave differently, suggesting that they are independent bands. The polarized component of the Raman band at 1452 cm^{-1} was downshifted by 24 and 9 cm^{-1} upon $^{18}O_2$ and d_4 substitution, but a depolarized band still remained there upon $^{18}O_2$ substitution, while it was shifted by 41 cm^{-1} upon d_4 substitution (spectra not shown). Therefore, it is likely that two bands are overlapped at 1452 cm^{-1}. The band at 1257 cm^{-1}, which is not seen upon excitation at other wavelengths, downshifts by 0 and 251 cm^{-1} upon $^{18}O_2$ and d_4 substitution, respectively, suggesting that its main component is C−H in-plane deformations. The Raman band at 819 cm^{-1} is markedly intensity-enhanced upon excitation at 351.1 nm.

Figure 5 shows the RR spectra of $BQ^{\bullet-}$ in MeCN (A) and water (B) excited at 325 nm. They are expected to gain RR intensity in resonance with an intense absorption around 310−320 nm in Figure 2 (third transition). The band at 1639 cm^{-1} gains intensity, while its counterpart at 1609 cm^{-1} loses

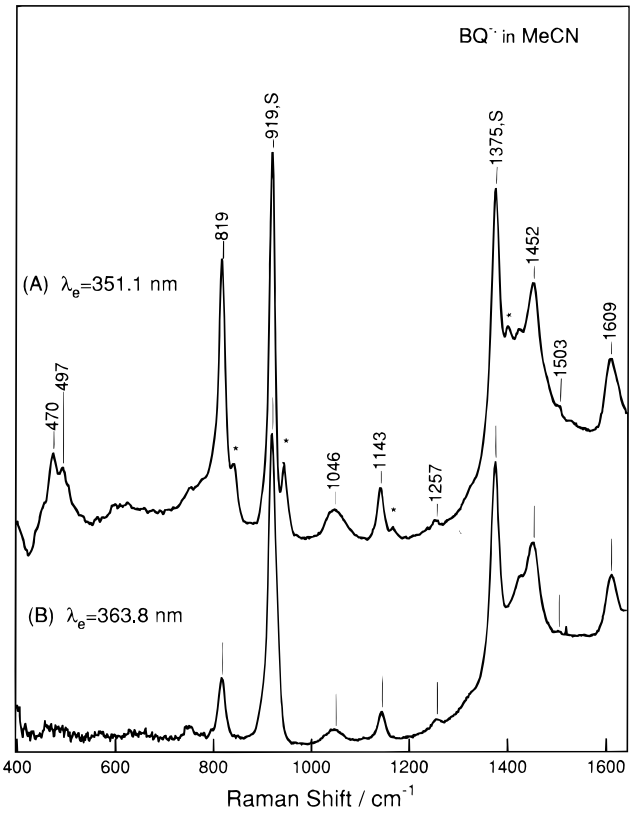

Figure 4. Resonance Raman spectra of $BQ^{\bullet-}$ in MeCN upon excitation at 351.1 (A) and 363.8 nm (B). The bands marked by S are solvent bands. Since another laser line separated by 24 cm^{-1} from 351.1 nm could not be completely eliminated from the excitation line, Raman bands excited by this line also appear in spectrum A, and such bands are marked by an asterisk. Laser power, 5 mW; accumulation time, 20 min.

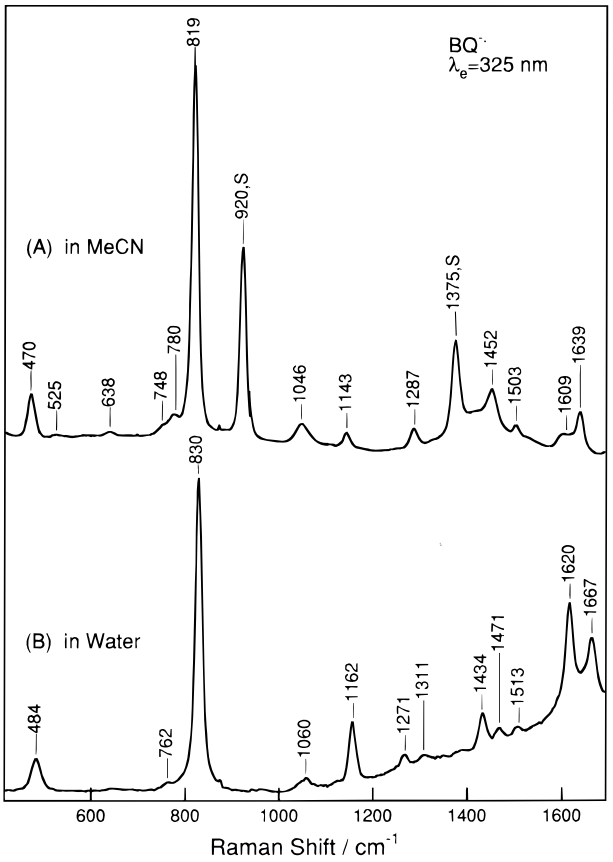

Figure 5. Resonance Raman spectra of $BQ^{\bullet-}$ in MeCN (A) and water (B) upon excitation at 325 nm. The bands marked by S are solvent bands. Laser power, 3 mW; accumulation time, 10 min.

intensity. In the low-frequency region, the band at 470 cm^{-1} is evident but its counterpart disappears. Some low-frequency modes at 525, 638, 748, and 780 cm^{-1} were barely recognized, and the bands at 1046, 1287, and 1503 cm^{-1} were very weak in the RR spectra excited at 351.1 and 441.6 nm (Figures 3 and 4). The band at 819 cm^{-1}, which was weak in the 441.6-nm excited spectrum, becomes most prominent in the 325-nm excited RR spectrum. In the spectrum of the aqueous solution, the band at 830 cm^{-1} is most prominent, similar to the case of the MeCN solution, but new bands appear at 1667 and 1471 cm^{-1}. It is stressed that the intensities of the RR bands at 819, 1143, and 1452 cm^{-1} relative to that at 1609 cm^{-1} are considerably different between the MeCN and water solutions at each excitation wavelength. These observations suggest that the geometrical structures of $BQ^{\bullet-}$ in the three electronically excited states corresponding to the absorptions around 448, 380, and 323 nm are significantly different.

Figures 6 displays the RR spectra of $BQ^{\bullet-}$ and its isotopomers in MeCN excited at 441.6 (A) and 325 nm (B), respectively. The 441.6-nm excited spectrum in the 1600-cm^{-1} region exhibits complicated patterns upon isotope substitution, but the patterns in the 325-nm excited spectra are rather simple; the two bands at 1609 and 1639 cm^{-1} shift to 1543 and 1576 cm^{-1} with d_4-$BQ^{\bullet-}$ and to 1595 and 1631 cm^{-1} with $^{18}O_2$-$BQ^{\bullet-}$. Therefore, they contain larger contributions from the C═C stretch and C—H deformation than the C═O stretch. In contrast, the Raman band at 1452 cm^{-1} is clearer in the 441.6-nm excited spectrum and exhibits a larger shift upon $^{18}O_2$ substitution ($\Delta\nu = 24$ cm^{-1}) than upon d_4 substitution ($\Delta\nu = 9$ cm^{-1}). In the 441.6-nm excited RR spectra, the prominent band at 1143 cm^{-1} shifts to 825 cm^{-1} upon d_4 substitution but returns to the original frequency upon $^{18}O_2$ substitution and is assigned to the C—H in-plane deformation mode. The band at 470 cm^{-1} exhibits a larger shift upon $^{18}O_2$ substitution ($\Delta\nu = 15$ cm^{-1}) than upon d_4 substitution ($\Delta\nu = 5$ cm^{-1}) and, accordingly, is considered to involve the in-plane C═O deformation mode.

In the 325-nm excited spectrum (Figure 6B), the band at 1503 cm^{-1} is shifted to 1322 cm^{-1} upon d_4 substitution but returns to 1497 cm^{-1} upon $^{18}O_2$ substitution. The most prominent band at 819 cm^{-1} shows a larger shift upon d_4 substitution ($\Delta\nu = 29$ cm^{-1}) than upon $^{18}O_2$ substitution ($\Delta\nu = 6$ cm^{-1}). The observed frequencies, depolarization ratio, and isotopic shifts and their suggested assignments are summarized in Table 2.

It is noted that when the RR spectrum of the $^{18}O_2$ derivative of $BQ^{\bullet-}$ was measured in $H_2{}^{16}O$, ^{18}O was replaced by ^{16}O so rapidly that we failed to observe the RR spectrum of $^{18}O_2$-$BQ^{\bullet-}$ in water, although such a phenomenon was not recognized for neutral BQ.[8] It took more than 2 weeks to prepare the 80% $^{18}O_2$-enriched BQ from a natural abundance of BQ in $H_2{}^{18}O$. The extremely rapid oxygen exchange with bulk water for $BQ^{\bullet-}$ implies that the interaction of the oxygen atom with bulk water is much stronger in $BQ^{\bullet-}$ than in neutral BQ.

The FTIR spectra of $BQ^{\bullet-}$ were seriously interfered by many strong bands of solvent and supporting electrolytes, and it was hard to reliably extract the contributions of solute from the observed spectra by difference calculations. Therefore, only clearly resolved IR bands are discussed in this paper. The frequencies, isotope shifts, and assignments of the observed IR bands are also listed in Table 2.

The protonated form of $BQ^{\bullet-}$ (i.e., $BQH^{\bullet}$) can be generated by UV laser photolysis of BQ in methanol[10,11] and is expected to give rise to an absorption around 270 nm.[27] Here the UVRR spectrum of $BQH^{\bullet}$ was obtained through excitation of BQ in

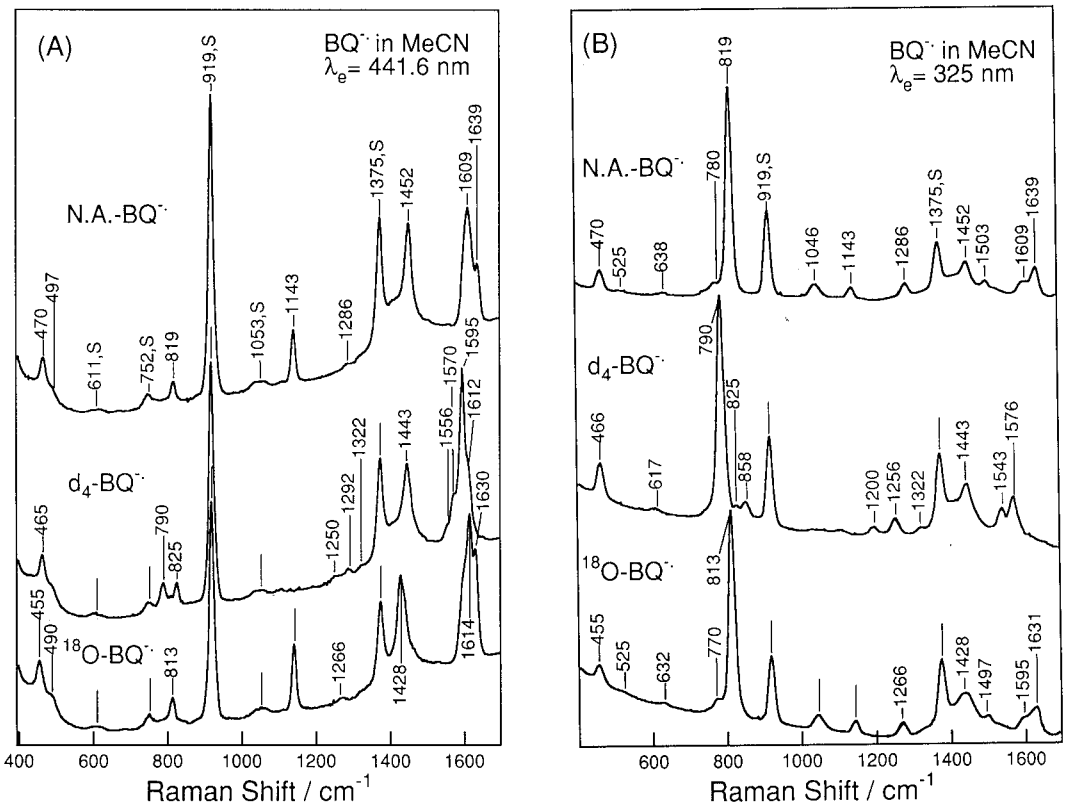

Figure 6. Resonance Raman spectra of $BQ^{\bullet-}$ and its $^{18}O_2$ and d_4-isotopomers in MeCN upon excitation at 441.6 (A) and 325 nm (B). The bands marked by S are solvent bands. Conditions for (A) and (B) are the same as those in Figure 3A and Figure 5A, respectively.

TABLE 2: Observed Frequencies, Isotope Shifts, Polarization Properties, Calculated Frequencies, and Band Assignments for $BQ^{\bullet-}$

obsd (in MeCN)				calcd			assignments		
ν	ρ^a	$\Delta\nu(^{18}O_2)$	$\Delta\nu(d_4)$	ν	$\Delta\nu(^{18}O_2)$	$\Delta\nu(d_4)$	sym.[b]	W^c	modes
		Raman							
1639	0.25	12	63	1638	12	58			$2\nu_1$
1614	0.25	13	322	1613	15	322			$\nu_{9a} + \nu_{6a}$
1609	0.25	14	66	1703	4	26	a_g, ν_2	ν_{8a}	ν(C=C) + δ(C−H)
1503	0.25	15	181	1513	15	192			$\nu_5 + \nu_{6a}$
1453	dp[d]	0[e]	41[e]	1490	0	41	b_{3g}, ν_8	ν_{8b}	ν(C−C) + δ(C−H)
1452	0.3	24	9	1522	26	10	a_g, ν_3	ν_{7a}	ν(C=O) + ν(C=C)
1286	0.25	20	30	1289	21	34			$\nu_{6a} + \nu_1$
1257	dp	0[e]	251[e]	1290	1	259	b_{3g}, ν_9	ν_3	ν(C−C) + δ(C−H)
1143	0.3	0	318	1181	0	327	a_g, ν_4	ν_{9a}	δ(C−H)
1046	0.3	0	188	888	0	219	b_{2g}, ν_{28}	ν_5	w(C−H)
819	0.25	6	29	838	6	29	a_g, ν_5	ν_1	ν(C−C)
780	0.3	10	138	878	10	139	b_{1u}, ν_{16}	ν_{18a}	ν/γ(C−C) + δ(C−H)
748	p[f]	0		826	1	82	b_{3u}, ν_{24}	ν_{17b}	w(C−H)
638	p	6	21	554	4	17	b_{2g}, ν_{29}	ν_4	w(C=O) + τ(chair)
525	p	0	*g*	517	1	96	b_{3u}, ν_{25}	ν_{16b}	w(C−H) + ν(C−C)
497	dp	7		484	8	23	b_{3g}, ν_{11}	ν_{6b}	γ(C−C−C) + δ(C=O)
470	0.3	15	5	468	15	4	a_g, ν_6	ν_{6a}	γ(C−C−C) + δ(C=O)
		IR							
1506		3	30	1593	0	26	b_{2u}, ν_{18}	ν_{19b}	ν(C=C) + δ(C−H)
1347		10	37	1412	12	34	b_{1u}, ν_{13}	ν_{19a}	ν(C=O) + ν(C−C)
780		10	138	878	10	139	b_{1u}, ν_{16}	ν_{18a}	ν/γ(C−C) + δ(C−H)

[a] Depolarization ratios. [b] Symmetry in D_{2h}. [c] Wilson mode for benzene derivatives; see ref 35 for the numbering. [d] Depolarized band. [e] The isotope shifts obtained in the RR spectra upon excitation at 363.8 nm (spectra not shown). [f] Polarized band. [g] The band shows a large downshift and is overlapped with other bands. Abbreviations: ν, stretch; δ, in-plane deformation; γ, ring deformation, ν/γ, a mixture of stretch and ring deformation; w, wag.

methanol by 10-ns pulses at 235 nm, and the Raman spectrum of a transient species, obtained by subtracting the contribution of neutral BQ from the observed spectrum (i.e., the difference between the high-power and low-power spectra) was regarded as the spectrum of $BQH^{\bullet}$. The RR spectrum of $BQH^{\bullet}$ (C) thus obtained as well as the raw spectra (A and B) is depicted in Figure 7. Only one prominent band (ν_{8a}) is observed at 1613 cm^{-1}, and this feature was the same as that for an aqueous solution (data not shown). This frequency agrees with that obtained in the RR spectrum excited at 417 nm,[28] but their spectral patterns are distinct. The strong intensity of the 1613-cm^{-1} band suggests that this molecule is distorted along the ν_{8a} mode in the 270-nm excited state, quite similar to the case of neutral BQ.[8]

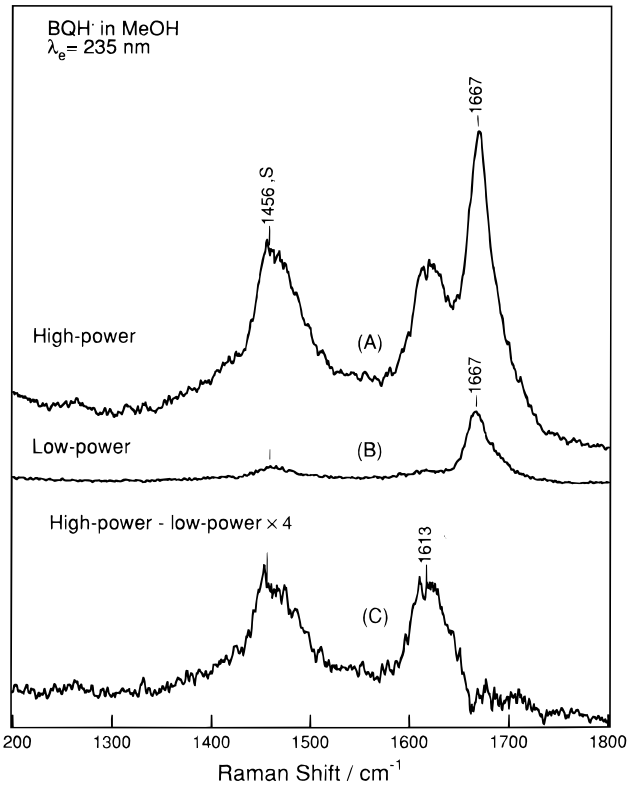

Figure 7. The 235-nm excited RR spectra of BQH• in methanol. Spectra A and B were observed with a higher laser power (50 μJ/pulse, 10 ns) and a lower laser power (5 μJ/pulse, 10 ns). Spectrum C denotes the difference, spectrum A − *k*[spectrum B]. Bands around 1456 and 1667 cm^{-1} are due to methanol and BQ in the ground state, respectively and *k* was determined to delete the 1667 cm^{-1} band in the difference spectrum. Accumulation time, 5 min.

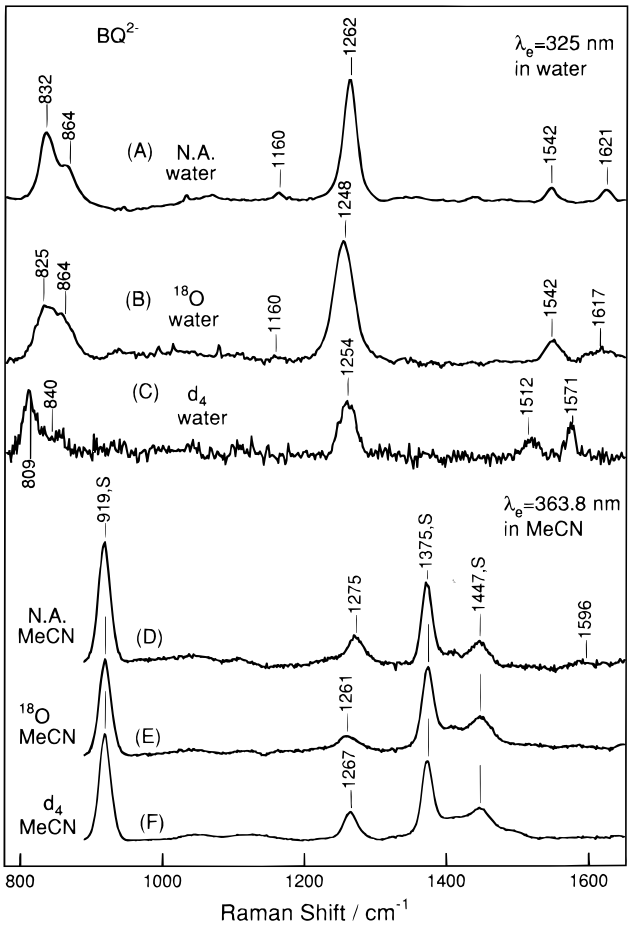

Figure 8. Resonance Raman spectra of BQ^{2-} in water excited at 325 nm (A−C) and that in MeCN excited at 363.8 nm (D−F). The bands marked by S are due to solvent. Spectra A and D, B and E, and C and F stand for natural abundance BQ^{2-}, $^{18}O_2$−BQ^{2-}, and d_4-BQ^{2-}, respectively. Laser powers, 3 mW for 325 nm and 5 mW for 363.8 nm. Accumulation times are 10 and 20 min, respectively.

Figure 8 shows the RR spectra of BQ^{2-} in water excited at 325 nm (A−C) and that in MeCN excited at 363.8 nm (D−F). BQ^{2-} is very stable at an extreme alkaline aqueous solution (pH > 13) under anaerobic conditions, presumably owing to a large stabilization energy through hydrogen bonds from water. Spectra A−C were obtained under such conditions. Since ^{18}O was easily replaced with bulk water, similar to the case of $BQ^{\bullet-}$, spectrum B was observed in $H_2{}^{18}O$. The most prominent band at 1262 cm^{-1} in spectrum A exhibits the largest $^{18}O_2$-isotopic frequency shift ($\Delta\nu$ = 14 cm^{-1}), and the bands at 832 and 1621 cm^{-1} show moderate $^{18}O_2$-isotopic shifts ($\Delta\nu$ = 7 and 4 cm^{-1}, respectively). This means that the C−O stretching mode is much more mixed with other benzene ring modes in BQ^{2-} than in the cases of $BQ^{\bullet-}$ and neutral BQ. On the other hand, BQ^{2-} is not stable in MeCN. In addition, the resonance enhancement of Raman intensity seems to be smaller for BQ^{2-} than for $BQ^{\bullet-}$. Accordingly, the quality of the RR spectrum of BQ^{2-} in MeCN is not as good as that of $BQ^{\bullet-}$, but bands are discernible at 1596 and 1275 cm^{-1} in spectra D−F excited at 363.8 nm. Frequencies, isotopic shifts in water, depolarization ratios, and plausible assignments of the observed RR bands of BQ^{2-} are summarized in Table 3.

The RR spectra of the protonated form of BQ^{2-} (i.e., BQH^-) and its isotopomers in water excited at 325 nm are shown in Figure 9. This RR spectrum is in preresonance with the first allowed electronic transition but is distorted by strong fluorescence. Nonetheless, some interesting features are noticed in Figure 9. The spectral pattern and band positions of BQH^- are quite similar to those of BQ^{2-} shown in Figure 8. The band at 1270 cm^{-1} exhibits the largest ^{18}O-isotopic frequency shift ($\Delta\nu$ = 12 cm^{-1}), and the bands at 1625 and 836 cm^{-1} show moderate shifts ($\Delta\nu$ = 4 and 5 cm^{-1}, respectively). The fact that the binding of a proton to BQ^{2-} has little effects on the vibrational frequencies of ring modes would suggest the attachment of a proton to a negative charge localized at the oxygen atom, i.e., binding of a proton to a practically nonbonding orbital. This is distinct from the case of protonation to $BQ^{\bullet-}$.

In order to assign the observed RR and IR bands qualitatively, unscaled *ab initio* MO calculations were performed as described in the Experimental Procedure section. Although detailed procedures and results will be given separately,[26] only the calculated results related to the vibrational assignments are presented here. The bond lengths of BQ, $BQ^{\bullet-}$, and BQ^{2-} optimized by the present calculations are given in Table 4. The calculated bond lengths for BQ and BQ^{2-} are in good agreement with the electron diffraction[29] and X-ray crystallographic data of BQ^{30-31} and BQH_2,[32] respectively. The C−O bond length is of a typical double bond for neutral BQ and of a typical single bond for BQ^{2-}, while that for $BQ^{\bullet-}$ is in between. Upon reduction of BQ to $BQ^{\bullet-}$ to BQ^{2-}, the C═C double bonds are elongated but the C−C single bonds are contracted, indicating that a quinoid ring changes to a benzenoid ring. This would mean that the extra negative charges of BQ^{2-} are mainly localized at two oxygen atoms and other π electrons are more delocalized among the six-membered ring.

These features qualitatively predict the directions of frequency changes of the C═O, C═C, and C−C stretches upon reduction of BQ to $BQ^{\bullet-}$ to BQ^{2-}, but for a more precise description, normal modes were also calculated. The calculated frequencies and isotopic frequency shifts are listed in Tables 2 and 3 together

TABLE 3: Observed and Calculated Frequencies, Isotope Shifts, Polarization Properties, and Band Assignments for BQ^{2-} and BQH^-

obsd (BQ^{2-})					calcd			obsd (BQH^-)		assignments		
ν(MeCN)	ν(water)	$\Delta\nu(^{18}O)$	$\Delta\nu(d_4)$	ρ^a	ν	$\Delta\nu(^{18}O)$	$\Delta\nu(d_4)$	ν	$\Delta\nu(^{18}O)$	sym.[b]	W^c	modes
1596	1621	4	50	p[d]	1658	2	24	1625	4	a_g	ν_{8a}	ν(C=C) + δ(C−H)
	1542	0	30	dp[f]	1537	0	30			b_{3g}	ν_{8b}	ν(C−C) + δ(C−H)
1275	1262	14	8	p	1323	21	8	1270	12	a_g	ν_{7a}	ν(C−O) + ν(C=C)
	1160	0	320	p	1175	1	312	1160	0	a_g	ν_{9a}	δ(C−H)
	832	7	23	p	845	7	42	836	5	a_g	ν_1	ν(C−C)
	494				472	16	5			a_g	ν_{6a}	γ(C−C−C) + δ(C−O)

[a] Depolarization ratios. [b] Symmetry in D_{2h}. [c] Wilson mode for benzene derivatives; see ref 35 for the numbering. [d] Polarized band. [f] Depolarized band. Abbreviations: ν, stretch; δ, in-plane deformation; γ, ring deformation; ν/γ, a mixture of stretch and ring deformation; w, wag.

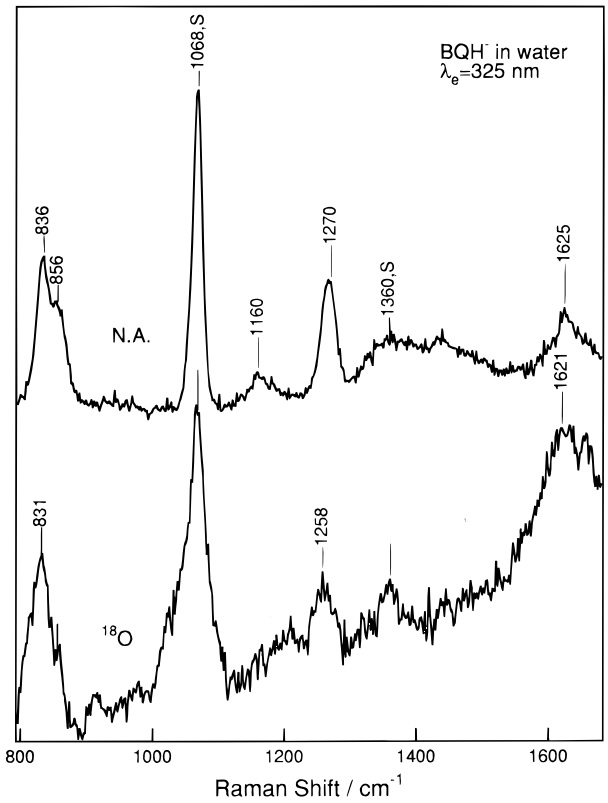

Figure 9. Resonance Raman spectra of BQH^- (upper) and its ^{18}O isotopomer (lower) in water excited at 325 nm. The bands marked by S are due to solvent. Laser power, 3 mW; accumulation time, 30 min.

TABLE 4: Experimental and Calculated Bond Lengths of BQ, $BQ^{\bullet-}$, BQ^{2-}, and BQH_2

	exptl			calcd[d]		
bond length	BQ[a]	BQ[b]	BQH_2[c]	BQ	$BQ^{\bullet-}$	BQ^{2-}
C=C	1.322	1.344	1.403	1.348	1.371	1.402
C−C	1.477	1.481	1.396	1.477	1.466	1.424
C=O	1.222	1.225	1.381	1.241	1.276	1.334
C−H		1.089	1.1	1.081	1.084	1.089

[a] X-ray crystallographic data from ref 31. [b] Electron diffraction data from ref 29. [c] X-ray crystallographic data from ref 32. [d] Calculated by *ab initio* MO method with the 631+G(d,p) basis set for oxygen atoms and 631G(d,p) basis set for other atoms.

with the observed values. All the calculated values given in Tables 2 and 3 are not scaled. It is noted that no noticeable frequency changes take place upon reduction of BQ for the C−H in-plane deformation vibrations. The gross charges on each atom and spin-density distributions of $BQ^{\bullet-}$ in the ground electronic state obtained in this calculation are given in parts A and B of Figure 10, respectively. The calculated spin densities, based on the natural orbial population analysis, are in reasonable agreement with the experimental data.[33,34]

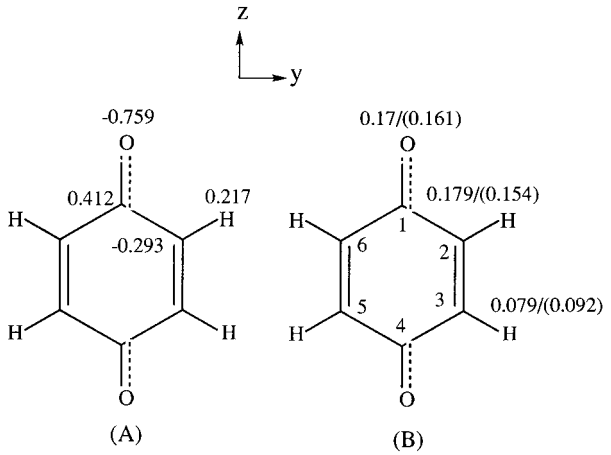

Figure 10. Calculated gross charges and spin density distributions for $BQ^{\bullet-}$. (A) Atomic partial charges calculated by GAUSSIAN 92. (B) Calculated spin densities. Numbers in parentheses denote the experimental values determined by refs 33 and 34.

Discussions

Assignments of the Fundamental Modes of $BQ^{\bullet-}$. If $BQ^{\bullet-}$ has D_{2h} symmetry in the ground state, the $3N - 6$ vibrational modes of $BQ^{\bullet-}$ are classified into

$$\Gamma = 6a_g + 5b_{3g} + 3b_{2g} + 1b_{1g} + 2a_u + 5b_{1u} + 5b_{2u} + 3b_{3u}$$

where the a_g, b_{3g}, b_{2g}, and b_{1g} species are Raman active and the b_{1u}, b_{2u}, and b_{3u} species are IR active (z: along C=O). Among them, the a_g, b_{3g}, b_{1u}, and b_{2u} modes arise from the in-plane vibrations. The vibrational spectra of neutral BQ have been satisfactorily interpreted in the D_{2h} framework.[6−8] In this approximation, only six totally symmetric modes should yield strong bands in the RR spectra excited at 441.6, 363.8, 351.1, and 325 nm. Since one of the six a_g modes is the C−H stretch, only five polarized bands are expected to appear strongly in the 300−1700-cm^{-1} region. Some of the bands assignable to nonfundamental modes may also appear in this region. Since no band which yields strong IR absorption appears in the RR spectra and vice versa (and, moreover, the fundamental RR bands, which are assigned to the group-theoretically-forbidden modes of the D_{2h} group are very weak) D_{2h} symmetry is applied for qualitative analysis and *ab initio* MO calculations of $BQ^{\bullet-}$ in the first approximation, and Wilson's mode numbering for substituted benzenes[35] will be used below.

On the basis of the observed $^{18}O_2$- and d_4-isotopic frequency shifts, the five prominent bands at 1609, 1452, 1143, 819, and 470 cm^{-1} in Figure 3 are assigned to the ν_{8a}, ν_{7a}, ν_{9a}, ν_1, and ν_{6a} fundamentals of the a_g species. The *ab initio* calculations (Table 2) fully support these assignments and give detailed descriptions of atomic motions involved in individual modes. These assignments are in line with Tripathi,[9] although the isotope shift data obtained here have made the assignments more

reliable. The polarized RR band at 1452 cm^{-1} is assigned to the in-phase C═O stretch (ν_{7a}), and the frequency of this mode for $BQ^{\bullet-}$ is significantly shifted from 1639 cm^{-1} of neutral BQ. The IR band at 1506 cm^{-1} was previously assigned to the C−O stretch,[14] but its $^{18}O_2$-isotopic frequency shift is only 3 cm^{-1} (see Table 2). It is more reasonable to reassign it to ν_{19b} of the b_{2u} species. In contrast, the band at 1347 cm^{-1} shows a larger $^{18}O_2$-isotopic shift (10 cm^{-1}), and the observed shifts upon $^{18}O_2$ and d_4 substitution are in good agreement with those calculated for ν_{19a}. The weak IR band at 780 cm^{-1}, which shows 10- and 138-cm^{-1} downshifts upon $^{18}O_2$ and d_4 substitution, is reasonably assigned to ν_{18a} of the b_{1u} species.

Three dp bands are discernible at 497, 1257, and 1452 cm^{-1} in Figure 4. There is no degeneracy in the electronic levels of $BQ^{\bullet-}$, and the electronic transitions around 400−280 nm are of the in-plane type. Therefore, it seems likely that the observed dp bands arise from b_{3g} modes. The band at 1452 cm^{-1} shows downshifts by 0 and 41 cm^{-1} upon $^{18}O_2$ and d_4 substitution, respectively, and it is reasonable to assign it to ν_{8b}. The normal coordinate calculations predicted the second b_{3g} mode (ν_3) at 1290 cm^{-1} and its $^{18}O_2$- and d_4-isotope shifts to be 1 and 259 cm^{-1}, respectively (Table 2). This agrees well with the observed features of the dp band at 1257 cm^{-1}, which shows 0- and 251-cm^{-1} downshifts upon $^{18}O_2$ and d_4 substitution, respectively. On the basis of the isotope shifts and calculated results, the band at 497 cm^{-1} is assigned to ν_{6b}.

Assignments of the Nonfundamental Modes of $BQ^{\bullet-}$. The complicated pattern in the 1620-cm^{-1} region in Figure 6A is due to the appearance of combinations and overtones, which interact with fundamentals through the Fermi resonance. The strong band of $BQ^{\bullet-}$ at 1639 cm^{-1} is downshifted by 63 and 12 cm^{-1} upon d_4 and $^{18}O_2$ substitution, respectively, which are in good agreement with the two corresponding isotope shifts of ν_1 (29 and 6 cm^{-1}, respectively). Both the 1639-cm^{-1} band and the ν_1 fundamental are strongly enhanced upon excitation at 325 nm. The ν_1 upshifts to 830 cm^{-1} in water (Figure 5), and the band in question also upshifts (to around 1660 cm^{-1}) in water. Accordingly, it is reasonable to assign the band at 1639 cm^{-1} to an overtone of ν_1. The $2\nu_1$ mode may interact with ν_{8a}. When $2\nu_1$ is shifted, the interaction with ν_{8a} may be deleted. This may be the reason why ν_{8a} becomes sharper in water upon excitation at 441.6 nm (Figure 6A). On the basis of the isotope shifts, solvent shifts, and excitation-wavelength dependence, the bands at 1614, 1503, and 1286 cm^{-1} (Figure 5) are assigned to $\nu_{9a} + \nu_{6a}$, $\nu_5 + \nu_{6a}$, and $\nu_1 + \nu_{6a}$, respectively, as summarized in Table 2 together with fundamentals. Interestingly, the frequency of the $2\nu_1$ band in MeCN is almost twice that of ν_1 but that in water is higher than the $2\nu_1$ frequency by 7 cm^{-1}. If the discrepancy arises from the anharmonicity of the potential, it would be caused by solvent−solute interactions, but the direction of deviation is opposite to general cases. This might be caused by some special interactions between $2\nu_1$ and other vibrations.

The relative intensities of the $2\nu_1$-to-ν_1 bands are 0.15 and 0.088 in MeCN and water, respectively. According to Gu and Champion,[36] the electron−nuclear coupling strength, S, is proportional to the ratio of the relative intensity of an overtone to its fundamental. If we assume that the shape functions of the Raman excitation profiles have remained unchanged between ν_1 and $2\nu_1$ in the MeCN and water solutions, S should be larger by a factor of 1.6 in water than that in MeCN. This may suggest that the relative absorption intensities of the 0−1 to 0−0 transitions should be larger in water than in MeCN. This agrees quite well with the observations shown in Figure 2.

Assignments of the Electronic Absorption Spectra of $BQ^{\bullet-}$. The controversy in the assignments of the absorption spectra of $BQ^{\bullet-}$ lies in whether the first excited state (∼440 nm) is $^2B_{3u}$ or ^2A_u and the third (∼320 nm) is $^2B_{1u}$ or a second excited state of $^2B_{3u}$ symmetry, although the assignment of the ground state to $^2B_{2g}$ has been established.[17−19] According to the resonance Raman theories, any vibrational fundamental, whose irreducible representation is contained in the direct product of the irreducible representations of the two excited electronic states, can be intensity-enhanced via vibronic coupling, but it should yield a dp band. As shown in Table 2, the dp bands observed upon excitation at 325, 351.1, or 441.6 nm, which are in resonance with the three lowest electronic transitions, are limited to b_{3g} modes. Since the second excited state has ^2A_u symmetry, a possible counterpart making b_{3g} vibrations vibronic active in the interaction with the second excited level should have B_{3u} symmetry. Therefore, the first excited state should be $^2B_{3u}$, and probably, the third excited state would also be $^2B_{3u}$ (second energy level of $^2B_{3u}$). This supports the recent *ab initio* calculations.

The two well-resolved absorption bands at 448 and 422 nm (Figure 2) were assigned to the vibronic progressions of ν_{8a} in the first $^2B_{3u}$ level. On the other hand, the splitting of the strong absorption band around 320 nm, which has a separation of ∼640 cm^{-1}, would also have a vibronic origin, but the responsible vibration would be ν_1 in this case. Interestingly, the absorption intensity of the 0−1 transition relative to that of the 0−0 transition is larger in MeCN than that in water for the ∼440-nm transition but vice versa for the ∼320-nm transition. The different solvent effects on the two vibrations (ν_1 and ν_{8a}) would cause differences in S for the two electronic transitions.

Vibrational Assignments of the RR Bands of BQ^{2-}. Under the assumption of D_{2h} symmetry for BQ^{2-} in the ground state, five a_g modes would be strongly enhanced upon excitation at 325 nm. As shown in the spectrum for the aqueous solution in Figure 8 and Table 3, the prominent band at 1621 cm^{-1} is polarized and shows 4- and 50-cm^{-1} downshifts upon $^{18}O_2$ and d_4 substitution, respectively. Therefore, it is reasonable to assign this to ν_{8a}. The prominent band at 1542 cm^{-1}, which is depolarized and shows 0- and 30-cm^{-1} downshifts upon $^{18}O_2$ and d_4 substitution, respectively, is assigned to an in-plane mode with b_{3g} symmetry. The calculated results predict that ν_{8b} is around 1537 cm^{-1} and shows 0- and 30-cm^{-1} downshifts upon $^{18}O_2$ and d_4 substitution, respectively. Accordingly, the 1542-cm^{-1} band can be assigned to ν_{8b}, and its intensity is gained through vibronic coupling in excited states. The strongest band at 1262 cm^{-1} shows 14- and 8-cm^{-1} downshifts upon $^{18}O_2$ and d_4 substitution, respectively. It also exhibits an upshift by 13 cm^{-1} in MeCN compared with that in water (Figure 8). This feature is assigned to a mode involving mainly the C−O stretch (ν_{7a}), and its frequency is sensitive to the presence or absence of hydrogen bonds to two oxygen atoms. The band at 1160 cm^{-1} shows a large deuteration shift ($\Delta\nu = 320$ cm^{-1}) and is assigned to ν_{9a}.

There are two prominent polarized bands appearing at 832 and 864 cm^{-1}. The *ab initio* calculations predicted only a single a_g mode (ν_1) in the region between 750 and 900 cm^{-1}. The stronger band (832 cm^{-1}) shows 7- and 23-cm^{-1} downshifts upon $^{18}O_2$ and d_4 substitution, respectively, as expected for ν_1. The weaker band (864 cm^{-1}) disappears upon d_4 substitution, while it shows no frequency shift upon $^{18}O_2$ substitution. Therefore, the weaker component of the doublet should be assigned to a combination or an overtone which obtains Raman intensity through Fermi resonance with ν_1. Similar to the case of the Fermi doublet of *p*-cresol,[37,38] it seems likely that the

stronger 832-cm^{-1} band arises from the ν_1 mode and the weaker counterpart arises from $2\nu_{16a}$ (out-of-plane ring deformation mode). When ν_{16a} is shifted upon deuteration, $2\nu_{16a}$ cannot interact with ν_1 and, therefore, loses Raman intensity. Although the attainable spectral quality for BQ^{2-} is much worse than that for $BQ^{\bullet-}$, we note that weak bands besides the four a_g fundamental modes also appear in the RR spectra.

Vibrational Assignments of the RR Bands of BQH^-. The molecular symmetry of BQH^- must be lower than D_{2h}. Nonetheless, the RR spectral pattern of BQH^- is very similar to those of BQ^{2-}, as shown in Figure 9. For convenience, the assignments of the Raman bands of BQH^- are discussed on the basis of D_{2h} symmetry, similar to $BQ^{\bullet-}$ and BQ^{2-}. The prominent band at 1625 cm^{-1} shows the $^{18}O_2$-isotope shift of 4 cm^{-1} similar to ν_{8a} of BQ^{2-} and is assigned to ν_{8a}. The strongest band at 1270 cm^{-1} shows a larger $^{18}O_2$-isotopic frequency shift (12 cm^{-1}). Accordingly, this is considered to contain mainly the C−O stretch (ν_{7a}). Assignments of other bands are similar to those of $BQ^{\bullet-}$ and BQ^{2-} as shown in Table 3.

Spectral and Structural Characteristics of Reduced Quinones. The *ab initio* calculations indicated that the C═O bond length becomes longer as the molecule is reduced, as shown in Table 4, and this change is reflected in the vibrational frequencies of ν_{7a}; the frequency changes from 1639 to 1452 to 1275 cm^{-1} in proceeding from BQ to $BQ^{\bullet-}$ to BQ^{2-}. The last frequency is close to that of a typical C−O single-bond-stretching mode. This means that the extra electrons in BQ^{2-} are mainly localized at the two oxygen atoms and occupy antibonding orbitals. In the case of $BQ^{\bullet-}$, it did not give two bands at 1639 and 1275 cm^{-1}, but a single ν_{7a} band is observed at an intermediate frequency. Therefore, the extra electron is delocalized between two oxygen atoms through an antibonding orbital with regard to the C═O bond.

In contrast, the ν_{8a} mode shows much smaller frequency shifts upon reduction; it shifts from 1666 to 1609 to 1596 cm^{-1} upon reduction from BQ to $BQ^{\bullet-}$ to BQ^{2-}. The amount of the frequency shift is significantly smaller for the second electron (13 cm^{-1}) than for the first one (57 cm^{-1}). In fact, the length of the C═C bond is calculated to be 1.402 Å for BQ^{2-} (Table 4), which is close to that of benzene (1.397 Å). Accordingly, the ν_{8a} frequency of BQ^{2-} is also close to that of benzene. The length of the C−C bond of BQ^{2-} is calculated to be 1.424 Å, which is appreciably longer than that of benzene, and thus, the ν_{8b} frequency of BQ^{2-} (1542 cm^{-1}) is lower than that of benzene. In this regard, the structural changes upon reduction of BQ obtained by *ab initio* calculations qualitatively agree with the observed features.

When $BQ^{\bullet-}$ is protonated, the negative charges on the oxygen atoms are deleted, and the π-electron distributions are affected by it. It may be approximated by a hole moving from the protonated oxygen to the other C═O, and as a result, the ν_{7a} largely upshifts, and ν_{8a} slightly downshifts, upon protonation to $BQ^{\bullet-}$. Since the negative charge on the oxygen atom is partial, the attached proton is not so stabilized, as the case of phenol, and therefore, its pK_a is less than 4.[39−41] In contrast, since negative charges are mainly located on two oxygen atoms in the case of BQ^{2-}, protonation to an oxygen atom scarcely perturbs the π-electron distributions of the benzene ring and the attached proton is sufficiently stabilized. As a result, the pK_a of BQH^- is larger than 13, and BQ^{2-} and BQH^- have similar structures and similar RR spectra.

In this way, a quinonoid ring is gradually converted to a benzenoid ring upon reduction from BQ to $BQ^{\bullet-}$, BQ^{2-}, and BQH_2. In accord with this, the ν_{8a} frequency decreases and the ν_{8b} frequency increases; the frequency separations between ν_{8a} and ν_{8b} are 293, 156, 79, and 14 cm^{-1} for BQ, $BQ^{\bullet-}$, BQ^{2-}, and BQH_2,[42] respectively, and this may serve as a measure of the extent of quinonoid character of the six-membered ring. We note that the Fermi doublet between ν_1 and $2\nu_{16a}$ appears around 810−860 cm^{-1} when the ring becomes benzenoid. According to *ab initio* calculations on $BQ^{\bullet-}$ and BQ^{2-}, ν_{16a} involves mainly out-of-plane displacements of the ring atoms but not of the oxygen atoms at the para positions. Therefore, its frequency is not sensitive to para substituents as well as to $^{18}O_2$ isotopes. When the ring becomes benzenoid, the $2\nu_{16a}$ frequency approaches the ν_1 frequency, and Raman intensity sharing with ν_1 through Fermi resonance takes place. In fact, Fermi doublets were observed for BQ^{2-}, BQH^-, and BQH_2 but not for BQ, $BQ^{\bullet-}$, and $BQH^{\bullet}$. Thus, the appearance of the Fermi doublet can also be used as a measure of the benzenoid character of the ring. As mentioned previously, the ν_{7a} (C═O stretch) frequency can also be used to distinguish between benzenoid and quinoid character. This band appears at ∼1640 cm^{-1} for a quinone ring (neutral BQ), at ∼1520 cm^{-1} for the semiquinoid form ($BQH^{\bullet}$), at ∼1450 cm^{-1} for the anion radical form ($BQ^{\bullet-}$), and at ∼1260 cm^{-1} for the benzenoid forms (BQ^{2-}, BQH^-, and BQH_2).

Symmetry Reduction and Geometrical Distortion of Solvated $BQ^{\bullet-}$. As shown in Figure 5 and Table 2, there are more than five polarized fundamental Raman bands in the frequency region below 1700 cm^{-1} in the RR spectra of $BQ^{\bullet-}$ excited at 325 nm. The extra bands, which cannot be assigned to nonfundamental bands as well as the a_g and b_{3g} fundamentals, include polarized bands at 525, 638, 748, 780, and 1046 cm^{-1} (Figure 5). This may suggest that either the ground state of $BQ^{\bullet-}$ is distorted from D_{2h} symmetry or impurities are present within these samples. Possible impurities include BQ, supporting electrolytes, photodimerized $BQ^{\bullet-}$,[43] and trace water in the electrochemical cell. However, all RR spectra, which were measured with different concentrations of supporting electrolytes, BQ, and trace water, with different solvents or with different laser powers, demonstrated that those bands were not due to contaminated impurities. Furthermore, the absorption spectra of $BQ^{\bullet-}$ shown in Figure 2 are in good agreement with the published spectra.[21,27] Consequently, it is unlikely that some impurities mixed with the $BQ^{\bullet-}$ samples gave additional RR bands.

On the other hand, one weak band of $BQ^{\bullet-}$ at 780 cm^{-1} (b_{1u}) appears in both the RR and IR spectra and shows the same isotope shifts in the RR and IR spectra upon $^{18}O_2$ and d_4 substitution (Table 2), indicating that $BQ^{\bullet-}$ has no center of symmetry. In addition, the bands assigned to the b_{3g} species are definitely depolarized. Therefore, the ground state of $BQ^{\bullet-}$ has an effective symmetry of either $C_s(\sigma_{xz})$ or $C_2(C_2(z))$. If the effective symmetry of $BQ^{\bullet-}$ in the ground state is C_2, the b_{1u}, b_{1g}, a_g, and a_u modes of D_{2h} would become the totally symmetric modes. The total number of b_{1g} and a_u modes is three, which is less than the number of extra observed bands. Furthermore, the *ab initio* calculations predicted that all b_{1g} and a_u modes are not sensitive to $^{18}O_2$ substitution. However, the band at 638 cm^{-1} shows a downshift by 6 cm^{-1} upon $^{18}O_2$ substitution. Thus, it seems unreasonable to assume that the effective symmetry of $BQ^{\bullet-}$ is C_2. The remaining possibility would be C_s with σ_{xz} (z, along CO; x, perpendicular to the benzene plane). Under C_s symmetry, the b_{2g}, b_{1u}, b_{3u}, and a_g modes of D_{2h} would become the totally symmetric modes. This may suggest small out-of-plane deformation in $BQ^{\bullet-}$. On the basis of the d_4- and $^{18}O_2$-isotope shifts and *ab initio* calculations, the bands at 1046, 748, 630, and 525 cm^{-1} are assigned to ν_5, ν_{17b}, ν_4, and ν_{16b}, respectively (Table 2).

The net charge distributions of gas-phase $BQ^{\bullet-}$ predicted by the *ab initio* calculations are shown in Figure 10. This would

be significantly altered in solution. For instance, the ν_{9a} frequency is higher by 19 cm^{-1} in H_2O than that in MeCN (1143 *vs* 1162 cm^{-1} in Figure 3), a fact which is most reasonably attributed to interactions of the four hydrogen atoms of $BQ^{\bullet-}$ with solvents. The solvation of $BQ^{\bullet-}$ may make the amount of charges (positive or negative) localized at all atoms larger than those in the gas phase.

According to the picture of the hydrogen bonding of the benzene ring with small molecules in the gas phase,[44−50] water molecules are located at the upper part of the quinone plane. Thus, the repulsive interaction between the protons of water molecules and C_1 or C_4 may make the disposition of the C═O group slightly out of the molecular plane. When this molecule is deformed from the planar structure, the Raman intensity would become weaker. If the intensity of ν_{8a} (C═C stretch) is regarded as standard, the intensities of ν_1, ν_{7a}, and ν_{9a} (relative to that of ν_{8a}) can be used to evaluate the approximate out-of-plane distortion of the quinone ring (C−C single bonds), C−O, and C−H groups, respectively. The relative intensities of these modes in water (3.8, 0.26, and 0.69, respectively) are appreciably smaller than those in MeCN (22.2, 0.61, and 1.1, respectively), suggesting larger nonplanar distortion in water than in MeCN, presumably owing to the cluster formation in water. According to the X-ray crystallographic structure,[51] $UQ_0^{\bullet-}$ (UQ_0: ubiquinone) definitely adopts nonplanar structures, and the discussion mentioned above predicts that the relative intensities of the ν_1 and ν_{7a} bands (to ν_{8a} band) are smaller than those of $BQ^{\bullet-}$ in MeCN. It was, in fact, as expected.[52]

Conclusions

Electrochemical RR spectroscopy of isotope-labeled BQ's combined with *ab initio* MO calculations has provided us with a clear description of the electronic structures, molecular structures, and bond properties of various reduced species of BQ. A few marker bands, which can characterize the strength of the C═O bonds and the nature of the six-membered ring, were pointed out for the first time. The ν_{7a} frequency, the separation between ν_{8a} and ν_{8b}, and the appearance of a Fermi doublet owing to ν_1 and $2\nu_{16a}$ all indicate that a quinoid ring gradually changes to a benzenoid ring upon reduction from BQ to $BQH^{\bullet}$, $BQ^{\bullet-}$, BQH^-, BQ^{2-}, and BQH_2. The C═O stretching frequency suggests that the extra negative charges of BQ^{2-} are highly localized at two oxygen atoms and the RR spectra of BQ^{2-} and BQH^- are alike, while an extra charge of $BQ^{\bullet-}$ is delocalized. These data would serve as basic information for analyzing the RR spectra of quinones observed for biological systems.

Acknowledgment. We thank Drs. Kiyoshi Tsuge, Hiroshi Nakajima, and Prof. Koji Tanaka of this institute for their help in electrochemical experiments and Drs. Y. Mizutani and T. Ogura of this laboratory for their help in measurements of the UV RR spectra. X. Z. thanks the Japanese Society for Promotion of Science for a postdoctoral fellowship. This study was supported by Grants-in-Aid for Scientific Research in Priority Areas (Molecular Biometallics) from the Ministry of Education, Science, Culture, and Sports, Japan, to T. K. (08249106).

References and Notes

(1) *The Chemistry of Quinonoid Compounds*; Patai, S., Ed.; John Wiley & Sons: New York, 1974. *Functions of Quinones in Energy Converting Systems*; Trumpower, B. L., Ed.; Academic: New York, 1982.

(2) Okamura, M. Y.; Feher, G. *Annu. Rev. Biochem.* **1992**, *61*, 881.

(3) Klinman, J. P.; David, M. *Annu. Rev. Biochem.* **1994**, *63*, 299.

(4) Ding, H.; Moser, C. C.; Robertson, D. E.; Tokito, M. K.; Daldal, F.; Dutton, P. L. *Biochemistry* **1995**, *34*, 15979.

(5) Breton, J.; Boullais, C.; Berger, G.; Mioskowski, C.; Nabedryk, E. *Biochemistry* **1995**, *34*, 11606.

(6) Becker, E. D. *J. Phys. Chem.* **1991**, *95*, 2818.

(7) Yamakita, Y.; Tasumi, M. *J. Phys. Chem.* **1995**, *99*, 8524.

(8) Zhao, X.; Imahori, H.; Sakata, Y.; Zhan, C.-G.; Kitagawa, T. *Chem. Phys. Lett.*, in press.

(9) Tripathi, G. N. R. In *Advances in Spectroscopy*; Clark, R. J. H., Hester, R. E., Eds.; John Wiley & Sons: New York, 1989; pp 157−218.

(10) Rossetti, R.; Brus, L. E. *J. Am. Chem. Soc.* **1986**, *108*, 4718.

(11) Beck, S. E.; Brus, L. E. *J. Am. Chem. Soc.* **1982**, *104*, 4789.

(12) Hester, R. E.; William, K. P. J. *J. Chem. Soc., Faraday Trans.* **1982**, *2*, 573.

(13) Terazima, M.; Hamaguchi, H. *J. Phys. Chem.* **1995**, *99*, 7891.

(14) Bauscher, M.; Mäntele, W. *J. Phys. Chem.* **1992**, *96*, 11101.

(15) Schuler, R. H.; Tripathi, G. N. R.; Prebenda, M. F.; Chipman, D. M. *J. Phys. Chem.* **1983**, *87*, 5357.

(16) Chipman, D. M.; Prebenda, M. F. *J. Phys. Chem.* **1986**, *90*, 5557.

(17) Tripathi, G. N. R.; Sun, Q.; Schuler, R. H. *Chem. Phys. Lett.* **1989**, *156*, 51.

(18) Wheeler, R. A. *J. Phys. Chem.* **1993**, *97*, 1533.

(19) Chang, H. M.; Jaffe, H.; Masmanidis, C. A. *J. Phys. Chem.* **1975**, *79*, 1118.

(20) Nakajima, H.; Kushi, Y.; Nagao, H.; Tanaka, K. *Organometallics* **1995**, *14*, 503.

(21) Morrison, L. E.; Schelhorn, J. E.; Cotton, T. M.; Bering, C. L.; Loach, P. A. In *Functions of Quinones in Energy Converting Systems*; Trumpower, B. L., Ed.; Academic: New York, 1982.

(22) Kaminaka, S.; Kitagawa, T. *Appl. Spectrosc.* **1992**, *46*, 1804.

(23) Charney, E.; Becker, E. D. *J. Chem. Phys.* **1965**, *42*, 910.

(24) Becker, E. D.; Ziffer, H.; Charney, E. *Spectrochim. Acta* **1963**, *19*, 1871.

(25) Frisch, M. J.; Trucks, G. W.; Head-Gordon, M.; Gill, P. M. W.; Wong, M. W.; Foresman, J. B.; Johnson, B. G.; Schlegel, H. B.; Robb, M. A.; Replogle, E. S.; Gomperts, R.; Andres, J. L.; Raghavachari, K.; Binkley, J. S.; Gonzalez, C.; Martin, R. L.; Fox, D. J.; Defrees, D. J.; Bakere, J.; Stewart, J. J. P.; Pople, J. A. *Gaussian 92*, Pittsburgh, 1992.

(26) Zhan, C.-G.; Iwata, S. To be published.

(27) Swallow, A. J. In *Functions of Quinones in Energy Converting Systems*; Trumpower, B. L., Ed.; Academic: New York, 1982.

(28) Tripathi, G. N. R.; Schuler, R. H. *J. Phys. Chem.* **1987**, *91*, 5881.

(29) Hagen, K.; Hedberg, K. *J. Chem. Phys.* **1973**, *59*, 158.

(30) Swingle, S. M. *J. Am. Chem. Soc.* **1954**, *76*, 1409.

(31) Trotter, J. *Acta Crystallogr.* **1960**, *13*, 86.

(32) Sakurai, T. *Acta Crystallogr.* **1968**, *B24*, 403.

(33) Das, M. R.; Fraenkel, G. K. *J. Chem. Phys.* **1965**, *42*, 403.

(34) Prabhananda, B. S. *J. Chem. Phys.* **1983**, *79*, 5752.

(35) Dollish, F. R.; Fateley, W. G.; Bentley, F. F. *Characteristic Raman Frequencies of Organic Compounds*; John Wiley & Sons: New York, 1974.

(36) Gu, Y.; Champion, P. M. *Chem. Phys. Lett.* **1990**, *171*, 254.

(37) Siamwiza, M. N.; Lord, R. C.; Chen, C. C.; Takamatsu, T.; Harada, I.; Matsuura, H.; Shimanouchi, T. *Biochemistry* **1975**, *14*, 4870.

(38) Takeuchi, H.; Watanabe, N.; Harada, I. *Spectrochim. Acta* **1988**, *44A*, 749.

(39) Adams, G. E.; Michael, B. D. *Trans. Faraday Soc.* **1967**, *63*, 1171.

(40) Wilson, R. L. *Chem. Commun.* **1971**, 1249.

(41) Rao, P. S.; Hayon, E. J. *J. Phys. Chem.* **1973**, *77*, 2274.

(42) Kubinyi, M.; Keresztury, G. *Spectrochim. Acta* **1989**, *45A*, 421.

(43) Gold, E. H.; Ginsburg, D. *J. Chem. Soc. (C)* **1967**, 15.

(44) Suzuki, S.; Green, P. G.; Bumgarner, R. E.; Dasgupta, S.; Goddard, W. A., III; Blake, G. A. *Science* **1992**, *257*, 942.

(45) Rodham, D. A.; Suzuki, S.; Suenram, R. D.; Lovas, F. J.; Dasgupta, S.; Goddard, W. A., III; Blake, G. A. *Nature* **1993**, *362*, 735.

(46) Perutz, M. F.; Fermi, G.; Abraham, D. J.; Poyart, C.; Bursaux, E. *J. Am. Chem. Soc.* **1986**, *108*, 1064.

(47) Brédas, J. L.; Street, B. G. *J. Am. Chem. Soc.* **1988**, *110*, 7001.

(48) Brédas, J. L.; Street, B. G. *J. Chem. Phys.* **1989**, *90*, 7291.

(49) Engdahl, A.; Nelander, B. *J. Phys. Chem.* **1985**, *89*, 2860.

(50) Atwood, J. L.; Hamada, F.; William orr, K. D. R.; Vincent, R. L. *Nature* **1991**, *349*, 683.

(51) Silverman, J.; Stam-Thole, I.; Stam, C. H. *Acta Crystallogr.* **1971** *B27*, 1846.

(52) Zhao, X.; Kitagawa, T. To be submitted.